An abrupt transition to an intergranular failure mode in the near-threshold FCG regime in Ni-based superalloys

J. Telesman, T.M. Smith, T.P. Gabb and A.J. Ring

NASA Glenn Research Center, Cleveland, OH 44135, USA

Abstract

Cyclic near-threshold FCG behavior of two disk superalloys was evaluated, and was shown to exhibit an unexpected sudden failure mode transition from a mostly transgranular failure mode at higher stress intensities to an almost completely intergranular failure mode in the threshold regime. The change in failure modes was associated with a crossover effect in which the conditions that produced *higher* FCG rates in the Paris regime resulted in *lower* FCG rates and increased ΔK_{th} values in the threshold region. High resolution scanning and transmission electron microscopy was used to carefully characterize the crack tips at these near-threshold conditions. Formation of stable Al-oxide followed by Cr and Ti oxides was found to occur at the crack tip prior to formation of unstable oxides. To contrast with the threshold failure mode regime, a quantitative assessment of the role that the intergranular failure mode has on cyclic FCG behavior in the Paris regime was also performed. It was demonstrated that the even a very limited intergranular failure content dominates the FCG response under mixed mode failure conditions.

Keywords: Superalloy fatigue crack growth threshold behavior; environmental degradation; intergranular failure; crack tip characterization; mixed mode failure

1. Introduction

Safe operation of gas turbine disks is enhanced by the use of damage tolerance methodology needed to meet engine certification requirements for rotating components. Of particular importance for achieving accurate damage tolerance life predictions is the ability to predict threshold fatigue crack growth behavior (FCG) which consumes the bulk of the crack growth lives. Yet some important aspects of the threshold FCG behavior in nickel-based turbine components are still not well understood.

In a recent publication (1) we reported on an unusual near threshold high temperature FCG behavior of two advanced nickel disk alloys. The paper detailed the so-called “crossover” effect in the near-threshold region where the conditions which produce higher FCG rates in the Paris crack growth regime can also produce higher resistance to crack growth in the near threshold regime (Fig. 1). While the unusual crossover effect in the threshold FCG region has

been reported previously by others (2-5), the most surprising finding was the identification of a sudden failure mode transition between the Paris regime and the near-threshold region. While the microstructural failure mode in the Paris regime was mostly transgranular, the failure mode changed abruptly to a fully intergranular mode at the low FCG rates of the threshold regime (Fig. 2). The intergranular failure mode transition in the near-threshold regime was documented to occur in the load shedding, K-decreasing type tests typically performed to determine the threshold stress intensity range (ΔK_{th}), as well as in the K-increasing constant amplitude tests when an abbreviated pre-crack test methodology was used to allow for commencement of the FCG tests at low stress intensities.

This sudden transition of failure modes in the near-threshold regime has not been previously reported. Further, existence of such a transition is rather surprising since the intergranular failure mode is typically associated with fast FCG rates and not the slow crack growth rates which define the threshold FCG region. The failure mode transition phenomenon was shown to be dependent on the environmental interactions between the air environment and the nickel-based alloys since it did not occur in tests conducted in vacuum, at lower temperatures or at high test frequencies, all of which limit either the amount of oxygen available to interact with a moving crack tip or decrease the rate of reaction occurring between the ambient environment and the crack tip region microstructure.

The primary goal of the original paper was to report, characterize and document this unexpected finding. The current paper will further examine the near-threshold regime failure mode transition phenomena based on additional work performed, which consisted of additional mechanical testing and a detailed characterization of the crack tip damage processes through the use of high resolution electron microscopy.

The cyclic FCG at the higher stress intensities, in the so-called Paris regime, typically also results in a limited amount of intergranular failure mode being present. In order to gain a better understanding of the differences between the near threshold intergranular failure mechanisms and those more commonly encountered during the mixed mode failure at higher crack growth rates, a detailed evaluation of the role that the intergranular failure plays in the mixed mode regime will also be presented.

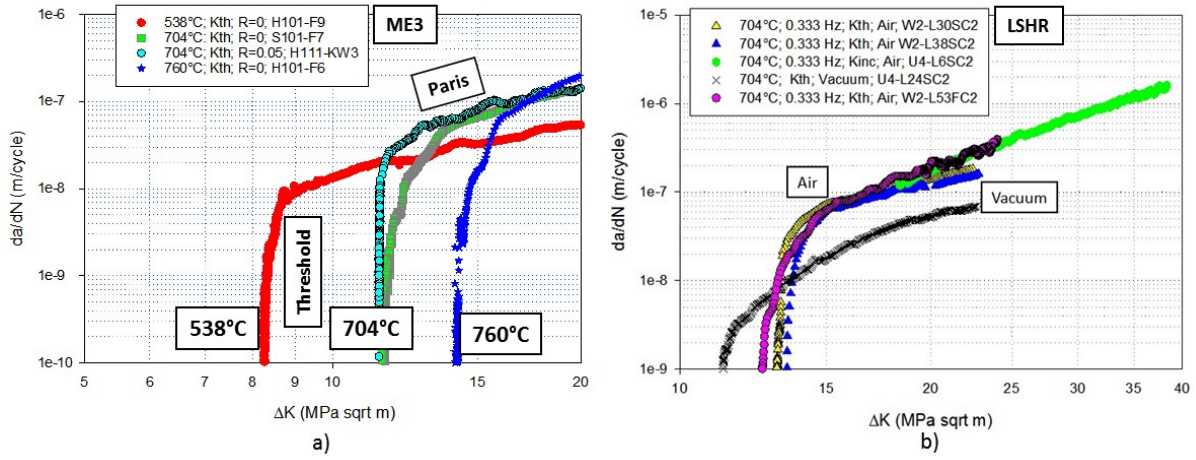

Figure 1. Load shedding, K-decreasing near threshold cyclic FCG results at 0.333 Hz showing the crossover effect between threshold and Paris regimes; a) ME3 at various temperatures, b) LSHR in air and vacuum at 704°C.

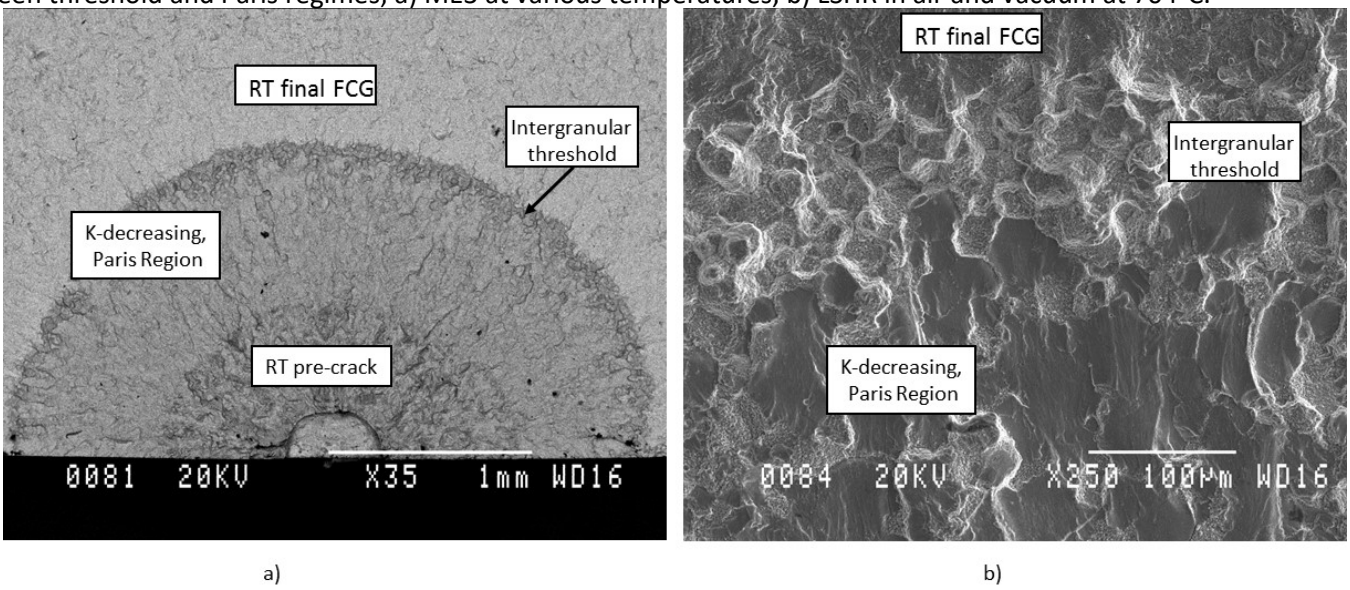

Figure 2. ME3 tested with load-shedding, K-decreasing; 704°C; 0.333 Hz: a) macroscopic view, b) sudden transition in failure modes.

2. Experimental

2.1 Materials and heat treatment

Blanks of forged LSHR and pancake forgings of ME3 disk alloys of compositions shown in Table I, were heat treated and given a two-step aging treatment. LSHR blanks were solution heat treated for 2 hours at 1171°C and aged at 855°C/4h plus 775°C/8h to achieve a supersolvus microstructure with an average grain size of approximately ASTM 8. Additional alternative heat treatments were used for specific tests on the LSHR alloy, which will be discussed in a later section. ME3 forgings were solution heat treated at 1171°C for 2 hours and aged at 843°C/4h

plus 760°C/8h to achieve a supersolvus microstructure with an average grain size of approximately ASTM 7.

Table I –Average Alloy Composition in Weight Percent

Alloy	Cr	Co	Al	Ti	Nb	Mo	Ta	W	Zr	B	C	Ni
LSHR	12.5	20.4	3.5	3.5	1.5	2.7	1.5	4.3	0.05	0.03	0.045	Bal
ME3	13	21	3.4	3.8	0.8	3.7	2.4	2.1	0.05	0.02	0.05	Bal

2.2 Fatigue crack growth testing

All crack growth testing was performed using the surface flaw, Kb bar specimen geometry with crack lengths measured by a computerized direct current electrical potential (DCEP) drop system. All specimens were pre-cracked at room temperature. Most of the testing was performed at 704°C in air with selected testing also done at 538°C and 760°C. To determine the effect of the environment, a small subset of tests was performed in a vacuum chamber at a 10^{-7} Torr pressure range. After room temperature pre-cracking, threshold testing was performed with the approximate initial stress intensity range (ΔK) of 24 MPa√m. Due to the geometry limitations imposed by the use of Kb bar specimens, a steep stress intensity shedding rate, C = -0.8 mm^{-1} , was utilized for the threshold tests. In order to obtain near-threshold FCG data without the use of a steep load shedding procedure, selected tests were pre-cracked to shorter crack lengths and the near-threshold data was acquired by conducting the test under constant stress range conditions which produced the more typical ΔK-increasing FCG curves.

2.3 Characterization of Cracks

Electron channel contrast imaging (ECCI) was performed on a high resolution Zeiss Auriga SEM focused Ion beam (FIB) using a back-scatter detector at 20kV with a 30um aperture. For STEM-EDS analysis, a FIB-TEM foil was produced using a FEI Helios Nanolab DualBeam 600 FIB. STEM-EDS was performed using a FEI Talos STEM at 200kV. The EDS maps were acquired using two Super-x EDS detectors and FEI VELOS software which has active drift correction. The Super-X EDX detection system utilizes two silicon drift detectors around the objective pole piece for improved collection performance. Maps were obtained using experimental K_α energies for Ni, Al, Cr, Ti, Co; L_α energies for Nb and Mo and M_α energies for Ta and W as their L_α energies correspond closely with the K_α energy of the Cu TEM holder.

3.0 Results

3.1 FCG Crossover Effects

For both the ME3 and the LSHR alloys, the load shedding threshold tests confirmed the presence of the crossover effect as shown in Fig. 1. Thus in the Paris regime of the ME3 alloy (Fig. 1a), the FCG rates increase as the temperatures rise, however in the threshold regime a

crossover occurs resulting in an increase in the threshold stress intensity, ΔK_{th}, with an increase in test temperature. At 538°C, the ΔK_{th} is approximately 8.2 MPa√m, 11.4 MPa√m at 704°C and 14 MPa√m at 760°C. For the LSHR 704°C load shedding, K-decreasing threshold FCG results for the LSHR alloy are shown in Fig. 1b. Here the major variable is the test environment, with multiple tests conducted in air compared to a vacuum threshold FCG test. As shown, the FCG rates in the Paris regime for the test conducted in vacuum were approximately three times slower in comparison to the similar tests conducted in air. The crossover effect is again evident with the vacuum test exhibiting faster near-threshold FCG rates and lower apparent ΔK_{th} than the tests conducted in air.

Effect of frequency was evaluated by performing a 704°C air threshold test on a LSHR specimen at 20 Hz. As shown in Fig. 3, the Paris regime FCG rates at 20 Hz were somewhat lower than for the 0.333 Hz, however the ΔK_{th} was much lower in comparison to the slower frequency thus again exhibiting the crossover effect. The threshold stress intensities, defined as the ΔK levels at the $1x10^{-10}$ m/cycle crack growth rate, were approximately 25%-30% higher at 0.333 Hz than for the test performed at 20 Hz. The near-threshold, K-increasing FCG test results were generally in good agreement (Fig. 4), while not identical, with tests conducted using load shedding, K-decreasing testing methodology. It should be pointed out that the short pre-crack tests were run at somewhat higher frequencies (0.667 and 2 Hz) than the 0.333 Hz used for load shedding tests.

To examine the influence of the load ratio on FCG behavior in the near-threshold region, a short pre-crack, K-increasing test was conducted at R=0.5 on a LSHR specimen tested at 704°C and 2 Hz frequency. The results, shown in Fig. 5, compare the FCG behavior as a function of the load ratio. It is clear that while the FCG curves for both R ratios merge at the applied stress intensities ΔK of 20 MPa√m or higher, the FCG rates diverge substantially in the low ΔK regime. Using a FCG value of $1x10^{-9}$ m/cycle as an indication of the approximate ΔK_{th}, threshold at R=0.5 is approximately one half of that at R=0.05. These large differences in ΔK_{th} due to the applied R ratios are typically ascribed (2) to differences in the extent of crack closure occurring in the crack wake and will be discussed later on in conjunction with formation of oxides in the crack tip region.

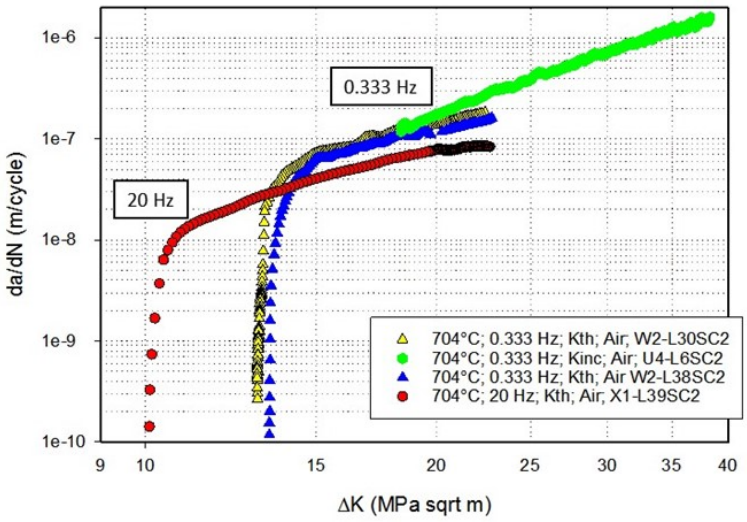

Figure 3. LSHR, effect of frequency on near-threshold behavior in tests done in air at 704°C.

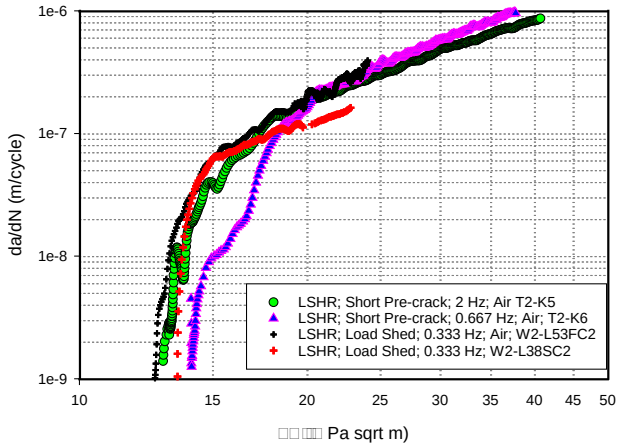

Figure 4. LSHR; comparison of near threshold FCG behavior for load shedding, K-decreasing and short precrack, K-increasing tests.

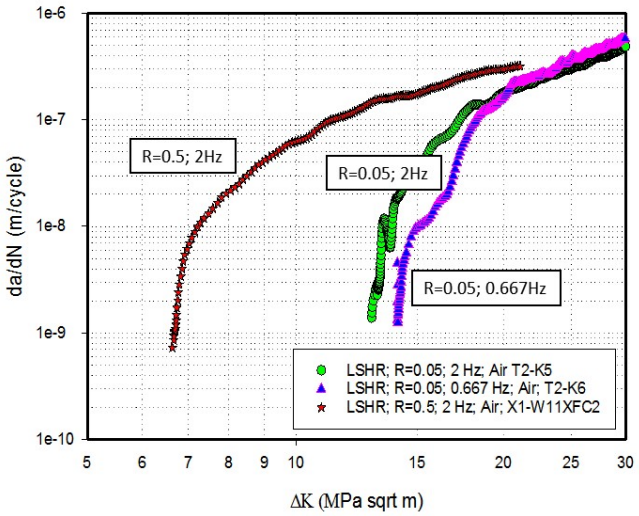

Figure 5. LSHR; Comparison of the near-threshold FCG behavior as a function of the R-ratio.

3.2 Intergranular Failure Mode

As has been described in detail in the recent paper (1), an unexpected transition in the failure mode occurred during FCG testing with a change from a mostly transgranular fatigue crack growth process in the Paris regime to a predominantly intergranular failure mode in the near threshold region of these two disk alloys. Examples of this observed sudden failure mode transition are shown in Fig. 2 and 6, with a more detailed characterization of the failure mode transition available in the above mentioned reference.

The optical images of the LSHR and ME3 load-shed threshold specimens tested at 704°C and shown in Fig. 6a and b, reveal that the intergranular threshold region is manifested by a thin dark ring encircling the entire Paris regime crack growth region. Also visible are the room temperature (RT) pre-cracking region, and the final room temperature crack growth region. Higher magnification scanning electron microscopy (SEM) images of the intergranular failure (Fig. 6c and 6d) reveal the region to be almost continuous with its width ranging approximately from 20 µm to 150 µm and spanning 1 to 6 grains. In contrast, the threshold test performed at 20 Hz did not undergo a failure mode transition and remained predominantly transgranular all the way through the threshold region (Fig. 7).

A typical appearance of a short pre-crack, K-increasing constant amplitude test is shown in Fig 8. This particular test was conducted on a LSHR specimen at 704°C and a 2.0 Hz frequency. As shown, after the end of the room temperature pre-cracking procedure, high temperature crack growth from the outset occurred by an intergranular failure mechanism. After approximately 130 µm of intergranular crack growth, the failure mode suddenly shifted and the cyclic crack growth continued by a mostly transgranular failure mode.

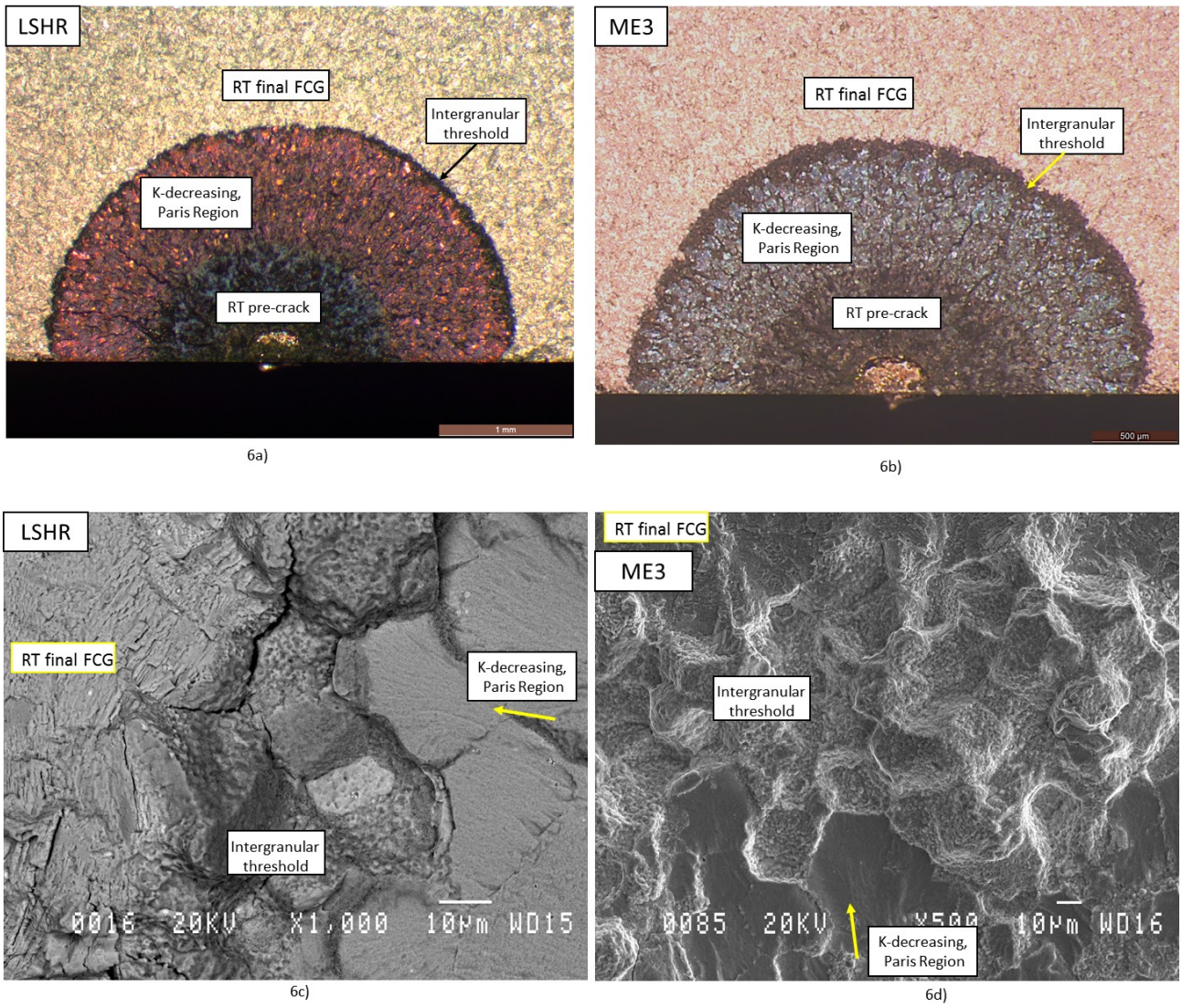

Figure 6. Optical and SEM micrographs of the fracture surface of the load shed, thresholds tests. Ring of intergranular FCG surrounding the Paris regime for 704°C tests of LSHR (a) and ME3 (b). Failure mode transition in a 704°C K-decreasing test performed at 0.333 Hz. Intergranular threshold width spans approximately 1 to 6 grains; c) LSHR and d) ME3.

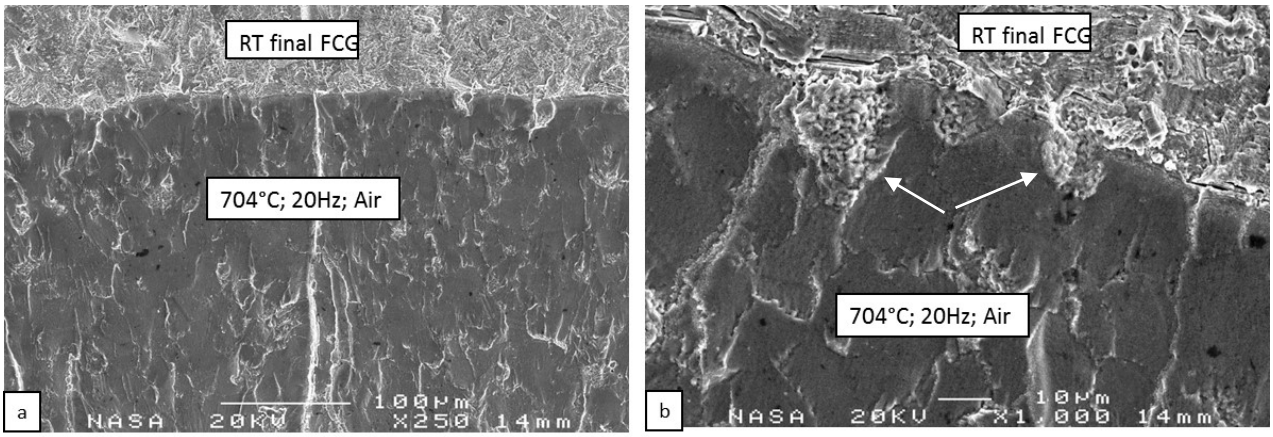

a) b)

Figure 7. LSHR; No extensive transition in failure modes for a 20 Hz K-decreasing threshold test performed in air (a). Small regions of intergranular failure visible at the lowest FCG rates measured at threshold, arrows (b).

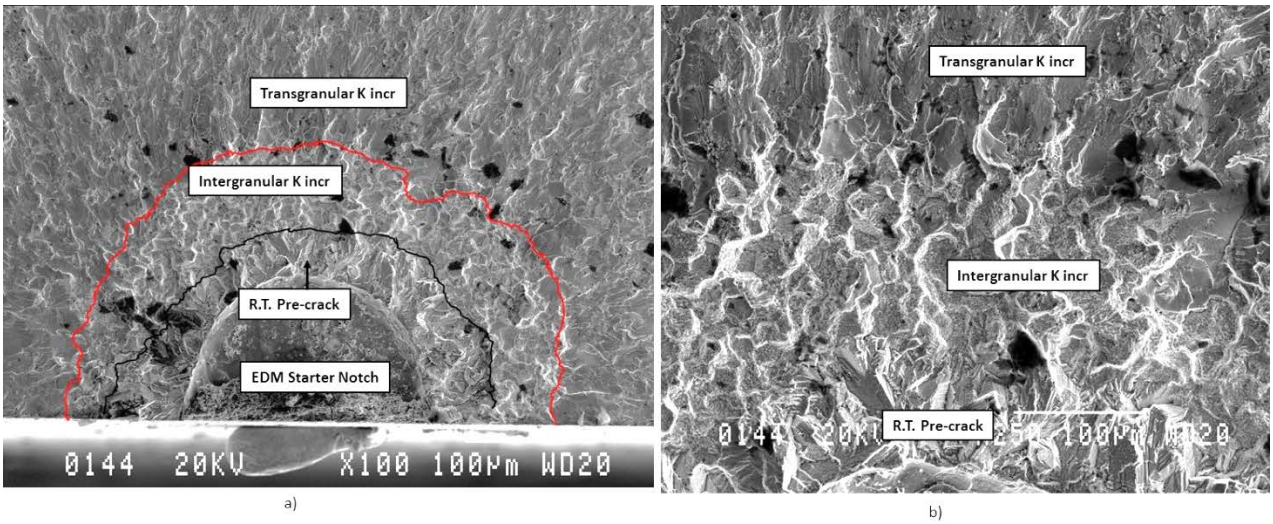

a) b)

Figure 8. LSHR short pre-crack, K increasing test at 704°C and 2Hz; a) lower and b) higher magnifications. An initial intergranular failure mode is followed by a sudden transition to a mostly transgranular failure.

The widths of the intergranular failure growth region, for the specimens tested at 704°C, are shown in Table II. Values shown are the average of five measurements. Significantly, the measured width of this region corresponds very closely to the crack length increments from the onset of the near-threshold regime, taken to be the change of slope away from the Paris region (approximately $4x10^{-8}$ m/cycle) to the end of the load shed threshold test as is detailed in Table II. This is also the case for the short precrack, K-increasing, tests for which the measurements are the width of the region taken from end of the precrack to the end of the intergranular region which is also shown in the Table. In addition, the corresponding maximum stress intensities (K_{max}) at which the transition in the failure modes occurred are also shown. The K_{max} transition values ranged from 13 to 18 MPa√m.

Table II. Comparison of Intergranular Band Width with Near-Threshold Region Crack Growth Distance - 704°C, Tested at R=0.05

Alloy/Specimen	Test Type	Frequency (Hz)	Crack length distance to/from $4x10^{-8}$ m/cycle to/from threshold (μm)	Avg. intergranular band width (5 measurements - μm)	Kmax at failure mode transition (MPa $m^{1/2}$)
LSHR/W2-L30SC2	Load Shed	0.333	75	72	14.5
LSHR/W2-L38SC2	Load Shed	0.333	75	82	14.5
LSHR/W2-L53FC2	Load Shed	0.333	187	170	15.5
ME3/H111-KW3	Load Shed	0.333	110	105	13
ME3/H111-KR3	Load Shed	0.333	120	110	13.8
LSHR/T2-K5	Constant Load/Short Pre-crack	2	137	131	15.8
LSHR/T2-K6	Constant Load/Short Pre-crack	0.667	205	222	18

3.3 ***Oxides***

The characterization of oxide thickness and composition in both the crack wake and at the crack tip region was conducted for two selected ME3 specimens.

Fig. 9 shows the changes in the oxide thickness and oxide morphology for a load shedding, K decreasing test, both in the Paris as well as the intergranular threshold regions. The measured values represent the oxide thickness on one half of the specimen. The most striking feature of this figure is the much thicker oxide layer of approximately 630 nm in the intergranular near-threshold region in comparison to the 260 nm oxide thickness in the mostly transgranular K-decreasing region. Since the K-decreasing test portion occurred prior to the onset of intergranular near-threshold behavior, it is clear that oxide formation is accelerated by the presence of grain boundaries in the near-threshold region. There is also a visible difference in the oxide morphology with the intergranular region exhibiting a much more irregular and jagged oxide appearance than the oxide present in the Paris regime.

In order to determine the key mechanisms by which intergranular near-threshold FCG takes place, an interrupted K-decreasing threshold test was performed. The purpose of this test was to identify active oxidation damage mechanisms at the crack tip by limiting the thermal exposure to prevent any additional oxidation of the crack tip area to take place. The test was performed at 704°C, at a frequency of 0.333 Hz and an R-ratio of 0.05. Once the cyclic FCG rates were well within the threshold regime, approximately $2x10^{-9}$ m/cycle, the test was interrupted and the furnace immediately turned off to limit the amount of time that the crack tip region was exposed to high temperature conditions. This specimen was sectioned and polished as a longitudinal section that bisected the semi-circular crack to perform high resolution

microscopy. As was previously described in the initial paper (1), the sudden failure mode transition from transgranular to intergranular occurred within the last 30-40 µm of the crack growth process (Fig. 10a, b and c). Oxide thickness as a function of the distance behind the crack tip was measured within the intergranular threshold failure region and is shown in Fig 10d. As shown, the full crack tip oxide thickness decreases rapidly in this region, changing from approximately 300 nm at a distance of 5µm from the tip to approximately 30 nm at a distance of 0.1 µm to 0.5 µm.

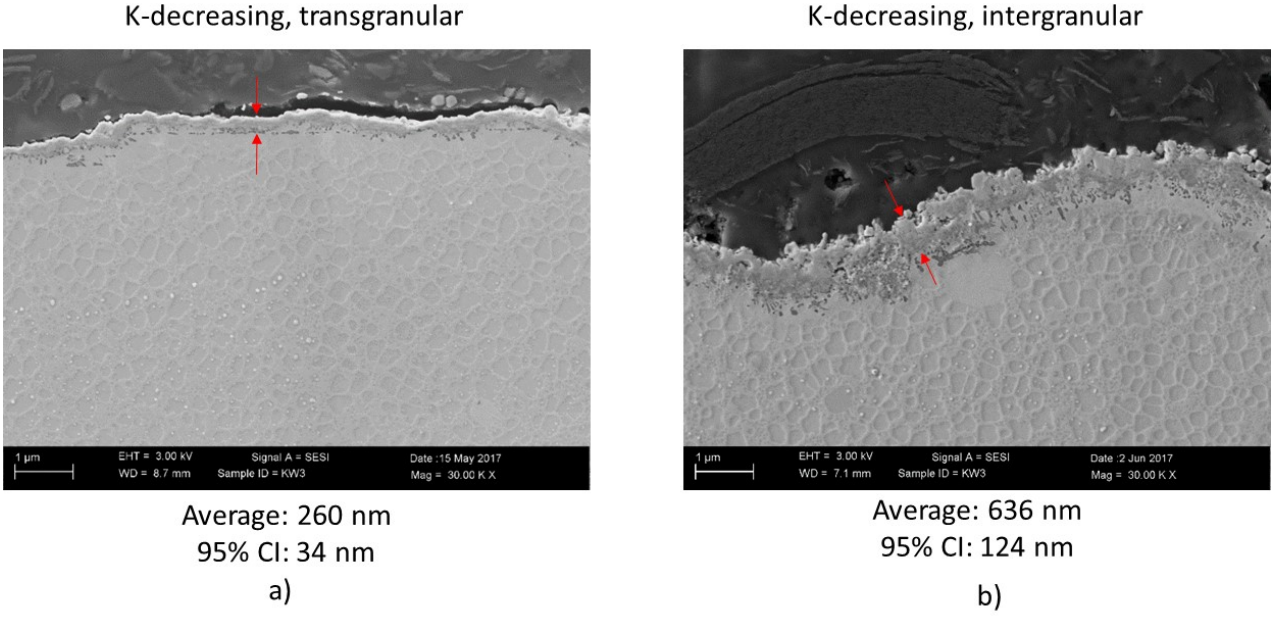

Figure 9. ME3; Measured oxide thickness (one half of the specimen) in the different segments of the test, (a) Paris - transgranular failure, (b) threshold – intergranular failure.

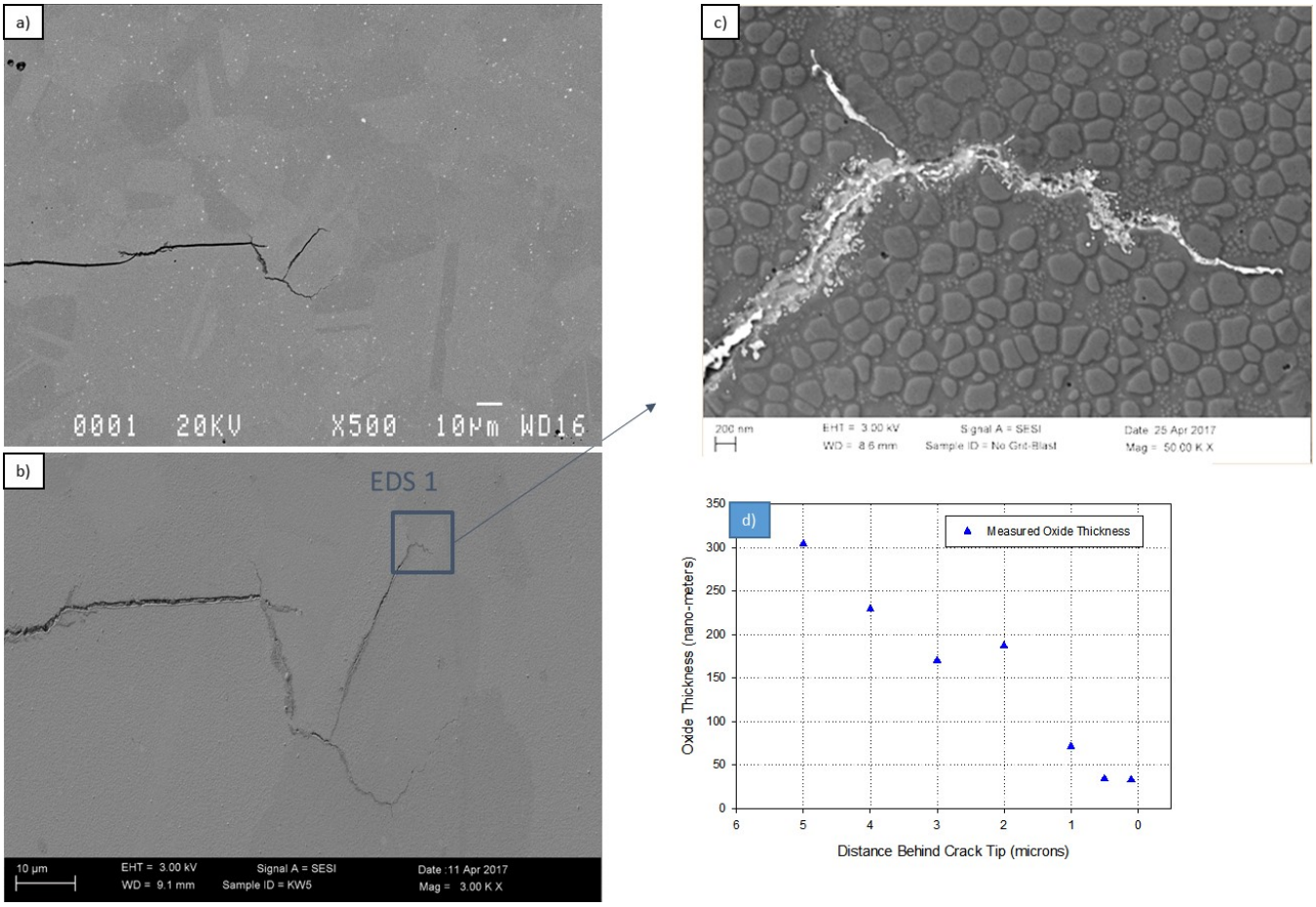

Figure 10. Failure mode transition, a) and b), crack tip oxide thickness image, c), and the oxide thickness measurement as a function of the distance behind the crack tip, d), in the interrupted ME3 test.

To quantify and characterize the nature of oxidation present near a crack tip, a FIB-TEM foil was produced as shown in Figure 11(a). The white rectangle represents the area extracted. The FIB foil region selected for analysis contains two areas of interest as detailed in the figure. The region labeled as “Grain Boundary Oxidation - A”, Fig 11b, contains a full secondary branch of an oxidized grain boundary which is assumed to be similar to the condition of the primary crack tip which was not available for analysis. The region labeled “Near Crack Tip - B” is an intergranular oxide region which is located very short distance behind the tip of a neighboring intergranular oxidized region.

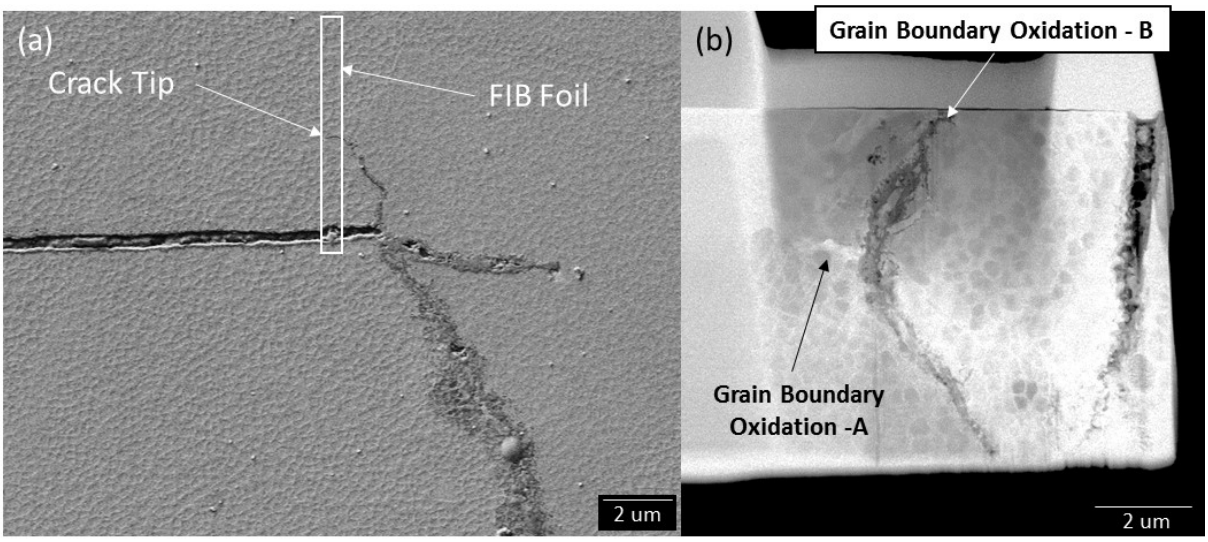

Figure 11. (a) A low-kV SEM image using an Everhart-Thornley detector of the crack that was analyzed in TEM. The rectangle box represents the area that was pulled for TEM analysis. (b) The TEM foil from (a) showing the two areas analyzed using high resolution EDS.

Figure 12 shows the EDS elemental maps taken from Grain Boundary Oxidation Region A. The very thin leading grain boundary oxide segment, (yellow ellipse: Figs. 12 a, b and g), consists of Al-oxide growing along the horizontal grain boundary. Behind the thin Al oxide segment is a wider and more developed intergranular region layered with Al oxides being present in the outer regions and Ti and Cr oxides layers in the inner regions (Figs. 12 c, d and g). Interestingly, also present among the grain boundary oxides are Ni and Co rich regions which have not as yet reacted with oxygen (red rectangles in Figs. 12 d, f and g).

A higher resolution composite image of the thin Al-oxide shown in Fig. 12 h, reveals a thin layer of γ (Cr, Co, Ni) between the Al-oxide and the γ’ precipitate. The white rectangle box in Fig. 12h denotes the area used to create the integrated line scan in Fig. 13. The scan confirms the presence of Al-oxide and shows the distribution of the other grain boundary elements as well as the composition of the adjacent γ and γ' regions.

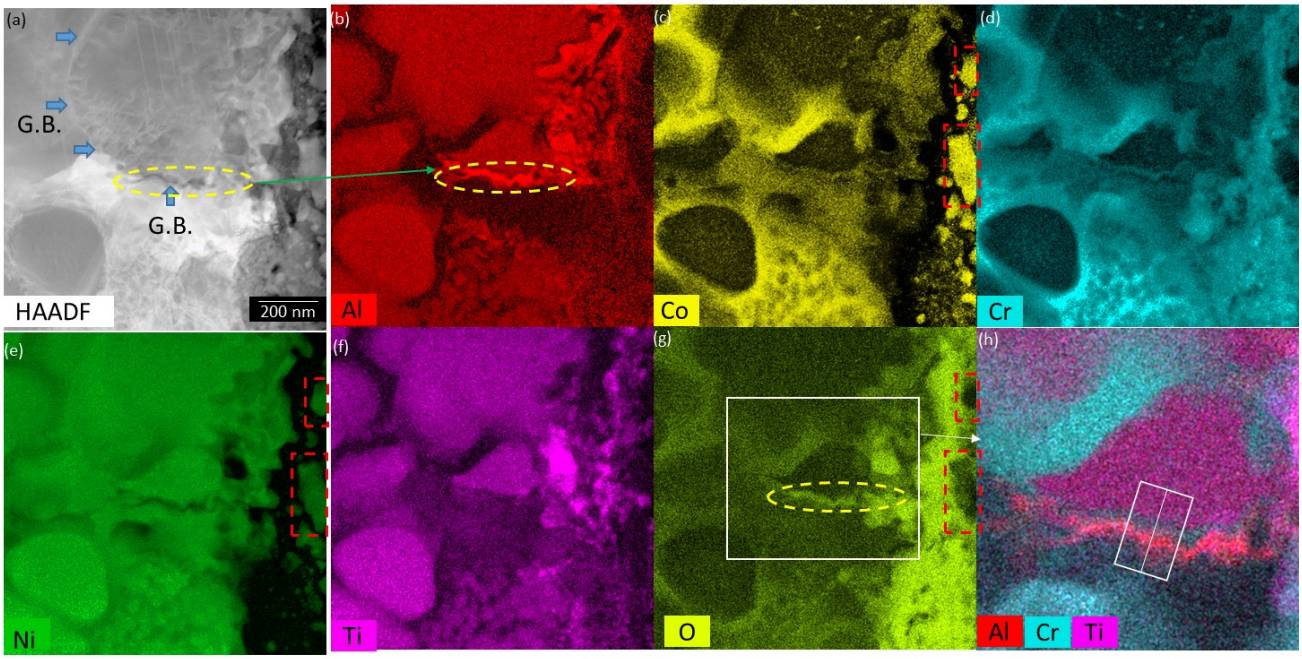

Figure 12. EDS elemental maps of oxidation along a grain boundary. The lower right image is a higher resolution composite image of the Al, Cr, and Ti maps revealing a layer of γ between the Al-oxide and the γ′ precipitate. The white rectangle box denotes the area used to create the integrated line scan in Figure 13.

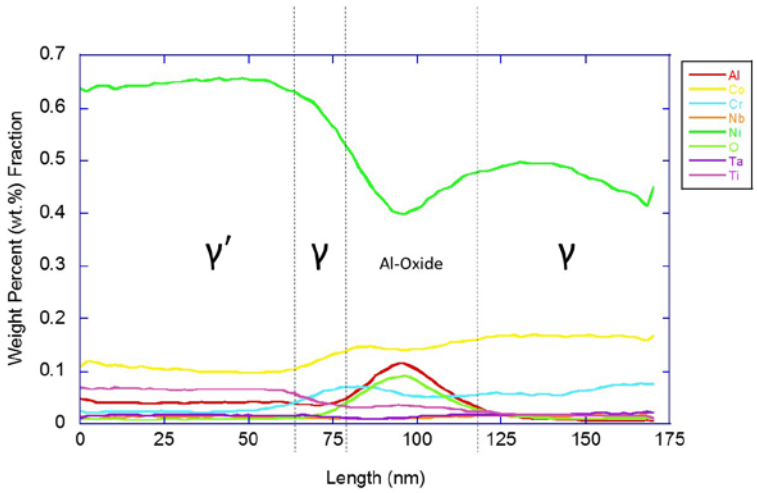

Figure 13. An integrated line scan revealing the weight percent of elements across the grain boundary.

Another notable observation in the Cr and Co elemental maps in Figure 12 is the presence of tertiary γ particles and stacking fault segregation observed in a γ′ precipitate at the top of the maps. Higher resolution EDS maps were taken of this area and are displayed below in Figure 14.

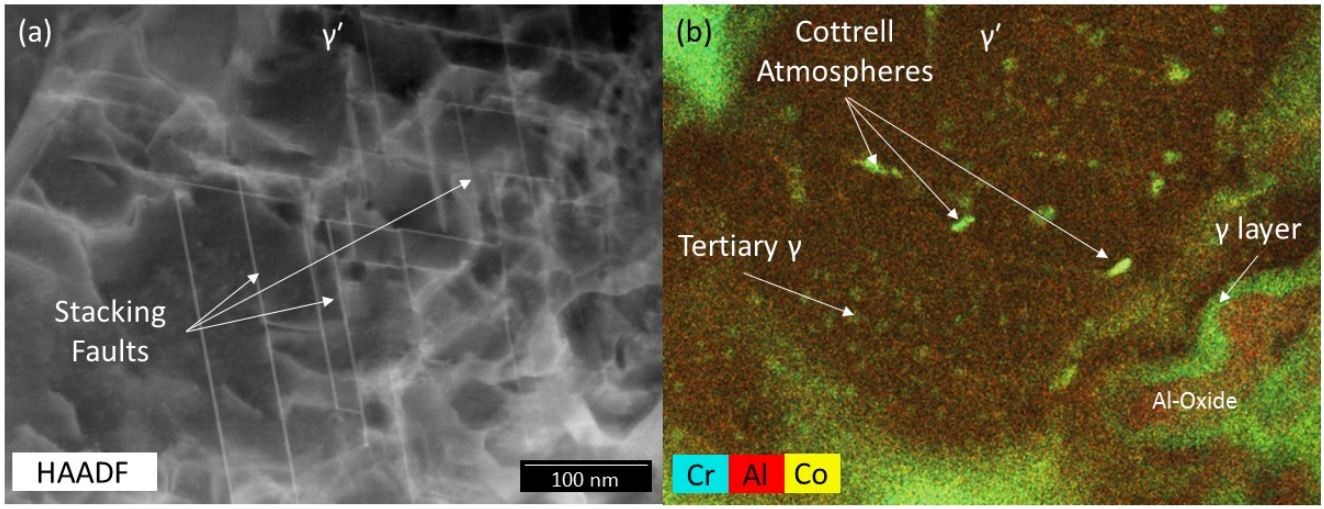

Figure 14. (a) A HAADF image of the deformation present in a γ′ precipitate near a crack as Al-Oxide enters from the right. (b) A composite net intensity map of Cr, Al, and Co revealing segregation along the stacking faults in the precipitate and tertiary γ particles present in the precipitate. A prominent layer of γ is observed ahead of the Al-oxide as it enters the precipitate.

Figure 14a is an HAADF-STEM image showing significant stacking fault shearing of a large γ′ precipitate near the crack with oxidation growing into it from the lower right. The stacking faults appear as bright lines in the HAADF-STEM image as they are being imaged "edge-on" on a <110} zone axis. In Figure 14(b) a composite image of the Cr, Al, and Co net intensity elemental maps is shown. A few notable observations can be made from this composite EDS map. First, the presence of tertiary γ particles can be observed embedded into the precipitate. The stacking faults are also highlighted by the Co and Cr maps revealing elemental segregation along them. This is significant as it proves that this diffusion-mediated process can occur at temperatures as low as 700°C and during fatigue deformation as well as creep. Additionally, the tertiary γ particles appear to have dissolved near the stacking fault segregation pointing towards these particles as possible sources of γ formers (Co and Cr) for this observed fault segregation. Finally, the presence of Al-oxide formation entering the precipitate can be observed in the lower right of the image. Indeed, as was observed in Figure 12 and 13, a layer of γ separates the Al-oxide from the adjacent γ′ precipitate.

The other area examined was the significantly oxidized Grain Boundary Region B, shown at the top of Fig 11b. High magnification HAADF and EDS map images of this region are shown in Fig 15. The morphology of the grain boundary consists mostly of oxidized particles formed in layers. While there appear to be voids between some of the oxidized particles, no conclusive statement can be made whether the oxidized grain boundary is cracked at this point. As shown, the oxidation behavior in this region is similar to that observed in Figure 12. In fact, Al-oxides

are observed at the outer edge of the oxide layer and entering into the microstructure, presumably attacking the secondary and tertiary γ' precipitates. The oxidation present inside the grain boundary appears to be dependent on the surrounding phase. If the oxide is near a secondary γ' precipitate, the oxidation primarily consists of Ti-oxides, whereas if the oxide is surrounded by the γ phase, Cr-oxides dominate. Moreover a clear depletion of Cr can be observed in the γ matrix surrounding the Cr-oxidation. Again, both Ni and Co present inside the grain boundary have not as yet been oxidized.

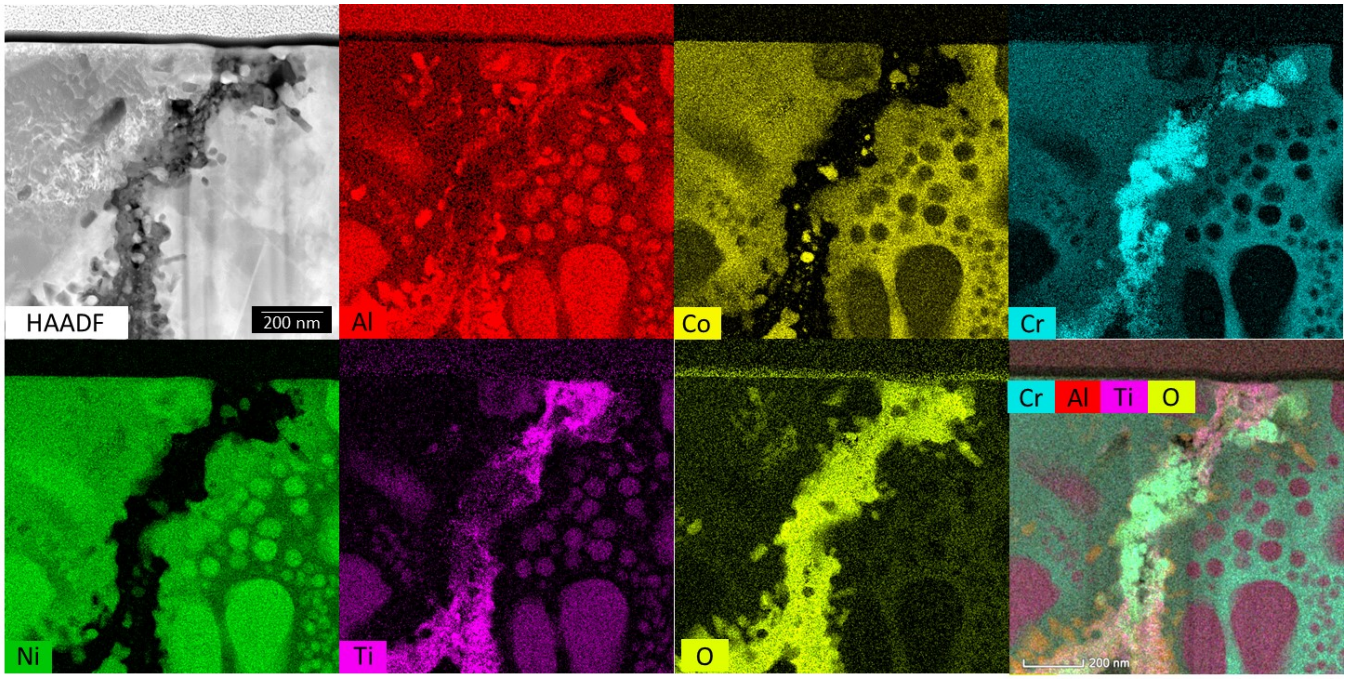

Figure 15. Grain Boundary Oxidized Region B. A HAADF-STEM image, top left, and the elemental maps of various grain boundary species. A composite of the net intensity maps for Cr, Al, Ti, and O shown in the lower right image.

4.0 Discussion

Two main issues arise in this study that must be explained: 1) the apparent slow fatigue crack growth rates associated with the intergranular failure mode in the near threshold FCG regime; and 2) the causes responsible for the sudden failure mode transition between the mostly transgranular Paris regime and the onset of intergranular failure. An important related question regarding the intergranular threshold FCG behavior is what type of a crack driving force is mainly responsible for crack extension?

In terms of past fatigue crack growth research in superalloys, a number of studies have shown that the type oxide formed at the crack tip has a pronounced influence on cyclic and dwell crack growth behavior (7-11). In particular it has been proposed that the formation of unstable and porous NiO at the crack tip significantly weakens and embrittles the grain boundaries causing fast intergranular crack growth rates (7, 11). However, as was demonstrated by Molins and

Andrieu (7, 9) by reducing the oxygen partial pressure or by increasing the Cr content, stable Cr_2O_3 oxide film can form at the grain boundaries without prior formation of nickel oxides. The chromia oxide film is well known to act as a protective barrier from further oxidation damage in general (12) and as was shown convincingly by Browning (11) in a study of IN718, it largely shields the crack tip from time dependent crack growth in nickel-based superalloys. It should be noted that most of this research was performed on IN718 which contains minimal amounts of Al and Ti.

Our STEM findings, based on the evaluation of the crack tip in the interrupted ME3 K-decreasing test, suggest that in the intergranular threshold regime, the oxidation process is considerably more complex than described above.

As described in Section 3.2, initially Al originating from the surrounding γ' precipitates begins to diffuse to the grain boundary forming Al-oxide. It's important to note that between this Al-oxide and the γ' precipitate is a layer of γ likely formed after aluminum diffused away from the precipitate. Eventually Al-oxides begin to branch out into the surrounding microstructure preferentially attacking the secondary and tertiary γ' precipitates. Once free surrounding Al has been depleted, Cr and Ti oxides begin to form depending whether the surrounding microstructure consists of γ or γ'.

An important finding regarding the intergranular oxidation sequence was the identification within the grain boundaries of Ni and Co rich regions in the non-oxidized state among the intergranular oxides already discussed. This finding was consistent for both intergranular regions evaluated and shown in figures 12 and 15. The lack of grain boundary nickel oxides points to the protective role that Al and Cr rich oxides play in protecting the crack tip region from the formation of these deleterious oxides. In this study, the presence of Ni oxides was confirmed for regions in the crack wake away from the crack which have been exposed at temperature for an extended time period. Thus the Ni oxides did not appear to be directly involved with crack tip oxidation or crack advancement. Therefore, the near-threshold oxidation process may be considerably different than the formation of unstable and porous NiO at the crack tip as has been identified by others (7, 10, 11) for conditions which led to accelerated intergranular FCG propagation.

Aluminum oxide, in the same manner as Cr-oxide, is also very stable and provides even a better barrier for oxygen diffusion, than Cr_2O_3 (13). Therefore at the very slow near threshold crack growth rates, a protective oxide layer can form at the crack tip to drastically slow down FCG by limiting the rate of oxygen diffusion ahead of the crack tip. The initial results pointing to the importance of aluminum oxide as the species contributing to the slow FCG in the near threshold region need to be confirmed. The observations have only been completed on one ME3 specimen. Work is underway on additional LSHR interrupted test specimens to confirm the existence of this mechanism and obtain a more detailed understanding of this crack tip process.

Regardless which crack tip oxide formation process is active, the formation of an oxide scale at the crack tip is still based on diffusion processes and thus is a function of time and temperature. As described earlier, a LSHR K-decreasing threshold test performed at a high frequency of 20 Hz in air did not exhibit the crossover effect (Fig. 3) and significantly, did not undergo a change in the failure modes (Fig. 7). Thus the cyclic near threshold FCG rates were too fast in terms of da/dt (m/s) to allow enough time to form the protective oxide layer.

4.1 Transition in the Failure Mode

The proposed need for a protective oxide film to exist at the crack tip in order to produce slow FCG rates can be used to explain the observed failure mode transitions. Cyclic FCG along grain boundaries should continue as long as kinetic reactions conditions favor formation of oxides at the grain boundaries. As was shown through the STEM work, aluminum oxide forms first followed by Cr and Ti oxides. Even these stable oxides will crack once their local fracture toughness is exceeded thus leading to crack growth. However, once the FCG rates become faster than the rate by which aluminum or chrome can diffuse to the crack tip, crack tip oxide formation becomes much more limited and cyclic plasticity driven transgranular crack growth mechanisms can become dominant. These are the same mechanisms which create transgranular FCG failure mode in vacuum tests.

Another factor which may be involved in determining the point at which the transition of failure modes occurs is the effect of a crack tip oxide film on the magnitude of cyclic plasticity driven dislocation motion. Mura (14) has suggested that a presence of an inert film can reduce elastic strain energy and improve fatigue life. Thus it is plausible that a presence of a stable crack tip oxide may produce the same effect and delay the onset of cyclic plastic deformation.

4.2 Crack Driving Force

The fundamental requirement for fatigue crack growth to occur in metals is for a critical level of crack tip cyclic plasticity to take place causing back and forth motion of dislocations. The dislocation damage accumulation at the crack tip due to the dislocation motion results in crack advancement. The magnitude of cyclic plasticity is controlled by the effective stress intensity range (ΔK_{eff}) which is based on the ΔK range over which the crack tip is open. The well-known oxide induced closure model (7) has been adopted by Yuen et. al. (2) for superalloys to explain both the crossover effect and the higher ΔK_{th} as the test temperatures are increased. The argument being that at higher temperatures, oxide thickness increases lowering the ΔK_{eff} and thus decreasing the resulting FCG rates. Nevertheless, the underlying assumption is that crack advancement is still occurring by the cyclic plasticity process. However it is very difficult to envision how a cyclic plasticity driven crack growth mechanism could result in an intergranular failure of oxidized grain boundaries or how cyclic plastic deformation could result in a transformation of failure modes. Yet, it is likely that the buildup of oxides in the crack wake and the subsequent spalling of some of the oxide particles due to repeated contact and rubbing played a role in influencing the FCG behavior by altering the crack driving force.

A recently proposed oxide formation threshold crack growth model by Chan (15) takes a considerably different approach of explaining time dependent thresholds in superalloys than the previously described oxide-induced crack closure approach. Of special interest is his crack growth criteria which is based on the determination whether the applied remote stress plus the local oxide induced transformation stresses result in a stress intensity at the tip, K_{tip}, which is greater than the local fracture toughness of the oxide, K_{ox}. If $K_{tip} > K_{ox}$ crack growth continues along the embrittled grain boundaries by micro-fracture, if not, time dependent crack growth is arrested.

It is well established that imposition of prolonged high temperature dwells at the maximum stress drastically increases the crack growth rates in terms of da/dN, by embrittling the crack tip and causing oxide assisted intergranular crack growth. For dwell crack growth tests, most of the crack growth occurs during holds and thus without the assistance of cyclic loading. Dwell crack growth data is usually plotted in terms of the K_{max} crack driving force parameter to reflect the predominance of crack advancement during hold time.

This poses an interesting question, what is the appropriate crack growth parameter to correlate threshold behavior since we have clear evidence of intergranular propagation occurring along heavily oxidized grain boundaries under cyclic conditions without the application of dwell cycles? To examine the question in more detail, the threshold FCG data presented in Fig. 5 was replotted in terms of the maximum applied stress intensity, K_{max} and is shown in Fig. 16. The original data shown in Fig. 5 exhibited considerably faster FCG rates and an approximate 50% reduction in the threshold stress intensity at R=0.5 in comparison to the R=0.05 test results. However when the same data is plotted in terms of the K_{max} parameter, the FCG rates for the various test conditions group closely together. These results indicate that the K_{max} parameter is an important contributor to the actual crack driving force parameter in the near threshold FCG region.

The ability of the Kmax parameter to correlate the FCG data in the intergranular threshold region is in agreement with brittle nature of the physical crack extension process which appears to occur by progressive micro-cracking of the grain boundary crack tip oxides. However a secondary influence of the cyclic ΔK parameter on the crack driving force is also likely by altering the shielding tractions in the crack wake due to spallation of the oxides and dislodging of particles which toughened the crack tip by interlocking and bridging of the two surfaces. Such processes are known to occur and influence stable crack growth in brittle monolithic ceramics (16). The extent by which these spalling type processes influenced FCG in the near-threshold region is unknown.

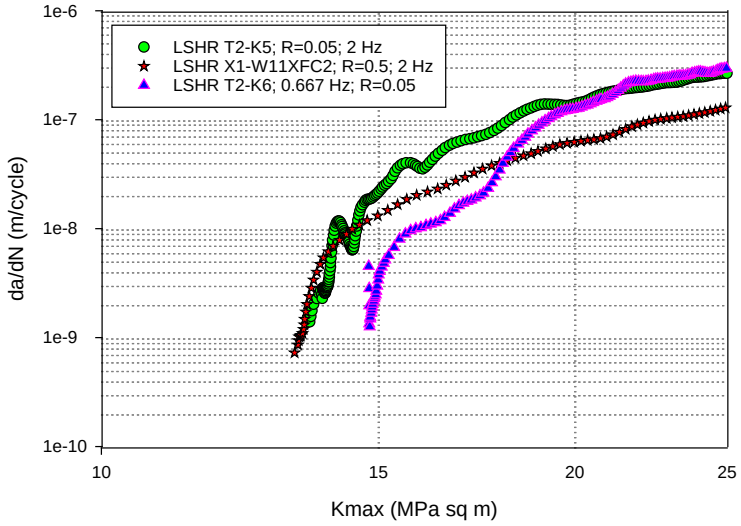

Figure 16. The use of Kmax parameter brought together the near threshold FCG rates of tests performed at R=0.05 and R=0.5 load ratios in the near-threshold region.

4.3 Role of Intergranular Failure in the Paris Regime

As has been discussed in detail in the previous sections, the presence and sudden transition to a fully intergranular failure mode in the near threshold cyclic FCG regime was unexpected. By contrasting the observed threshold behavior with the FCG failure modes observed in the Paris regime, a deeper understanding of the relationship between microstructural parameters, test environment and the associated cyclic fatigue crack growth behavior can be obtained.

Typical descriptions of the operative failure modes in cyclic FCG testing of superalloys at temperatures of 600°C and above, is that of a mixed mode failure which implies presence of both transgranular and intergranular failure modes. However, it is not at all clear how these different co-existing failure modes impact the cyclic FCG rates. It has been generally accepted that the intergranular failure mode in the Paris regime is a result of environmental degradation which can occur at certain grain boundaries which are more prone to environmental damage.

The Paris regime FCG results of the LSHR alloy tested as part of this study as well results from a more extensive earlier companion study of the same alloy (17), are in agreement with the expected trends. FCG testing was conducted in air at 704°C for various frequencies ranging from 0.333 Hz all the way up to 30 Hz, and compared to vacuum tests to isolate the effect of environment with the results shown in Fig. 17a. The FCG data shows that as the frequency is increased, the crack growth rate decreases and begins to approach the FCG rates measured in vacuum. The differences between the air and vacuum FCG rates are largest at the lower applied stress intensities and thus in the regime where the crack growth is slowest. At higher frequencies and stress intensities, the fatigue crack growth rates produced for tests conducted in air were indistinguishable from the vacuum fatigue crack growth rates. All these trends can be explained by considering that a competition exists between the diffusion rate of the

embrittling species, in this case oxygen, and the rate of FCG. If the crack growth rate is faster than the diffusion rate of the embrittling species, the environmental degradation is eliminated and the FCG behavior becomes indistinguishable from that of tests conducted in vacuum.

It is important to realize how different these trends are than those exhibited in the near threshold intergranular failure regime. The lower ΔK region of the Paris regime is the most susceptible to environmental effects due to the slower FCG rates (Fig. 17a). Thus decreasing the test frequency to 0.333 Hz resulted in approximately three times faster FCG rates than the high frequency tests. However in the near threshold intergranular failure mode region, at even slower FCG rates, the trends are reversed with the test conducted at the slower frequency of 0.667 Hz producing slightly lower crack growth rates than the 2 Hz test (Fig. 4).

The role of the test frequency on FCG behavior is most clearly demonstrated in an additional test which was performed as part of the Paris regime study. In this case, a K-increasing test was started at a frequency of 10 Hz and after substantial amount of crack growth, the test was transitioned to 0.333 Hz at a ΔK of 25 MPa√m. As shown in Fig. 17b, the FCG rates increased immediately by approximately 2.3 times after the change in frequency. Also as shown, the FCG rates measured in this test were in full agreement with the baseline FCG data of other specimens measured at both of these frequencies, thus indicating that no synergistic frequency interactions took place.

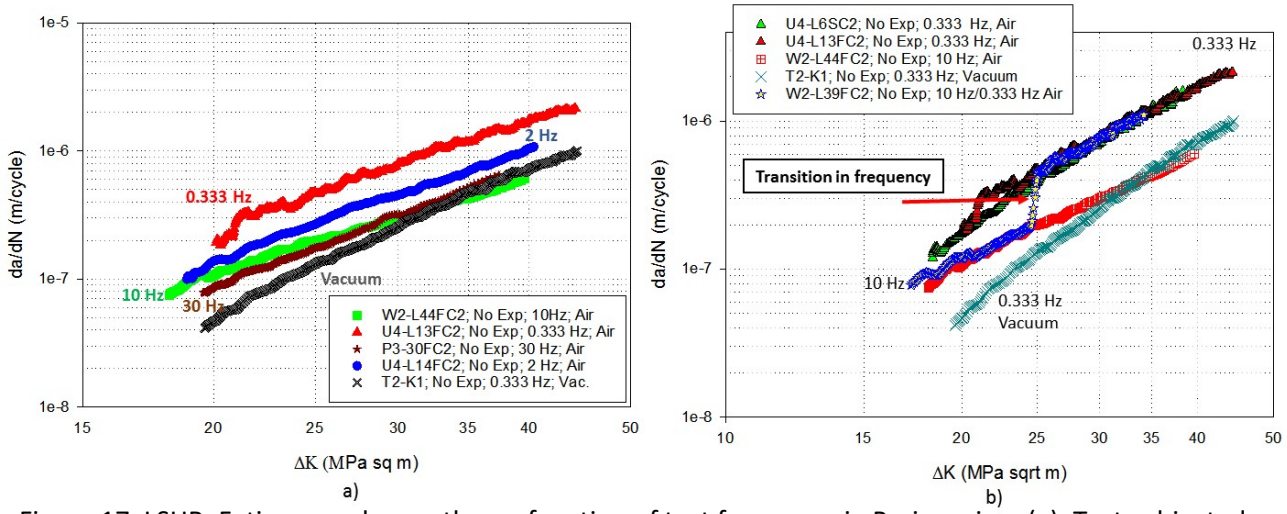

Figure 17. LSHR; Fatigue crack growth as a function of test frequency in Paris regime (a). Test subjected to a mid-stream change in frequency from 10 to 0.333 Hz produced a large shift in FCG rates (b).

However the most pertinent aspect of this frequency transition test was the observation that there was noticeable increase in the amount of intergranular failure after the transition to the lower frequency. In order to obtain a quantitative analysis of this finding, a small test program was devised. A test was performed on an LSHR specimen at 704°C using a constant ΔK of 25 MPa√m at R=0.05. The test consisted of three constant ΔK segments performed sequentially at 10 Hz, 0.333 Hz and 2 Hz. This produced significant constant ΔK crack length segments to allow

for a quantitative assessment of the percentage of intergranular failure. For each frequency, three to five SEM images obtained at 1000x magnification were analyzed using Adobe Photoshop CS3 software to map and quantify the percentage of intergranular and transgranular failure modes present on the image. Fig. 18 provides examples of this procedure.

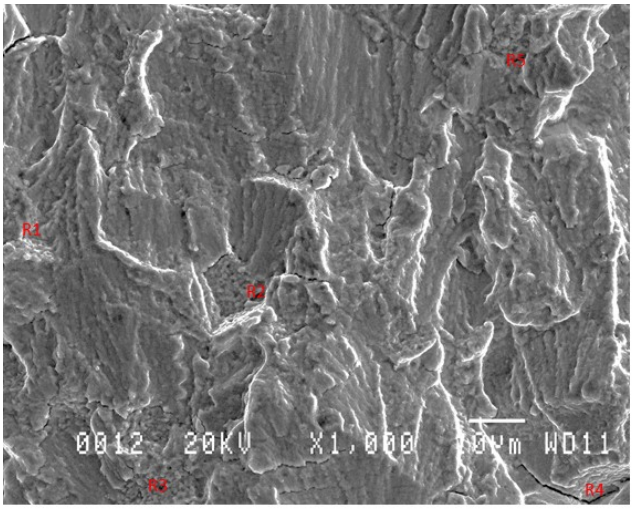

18a)

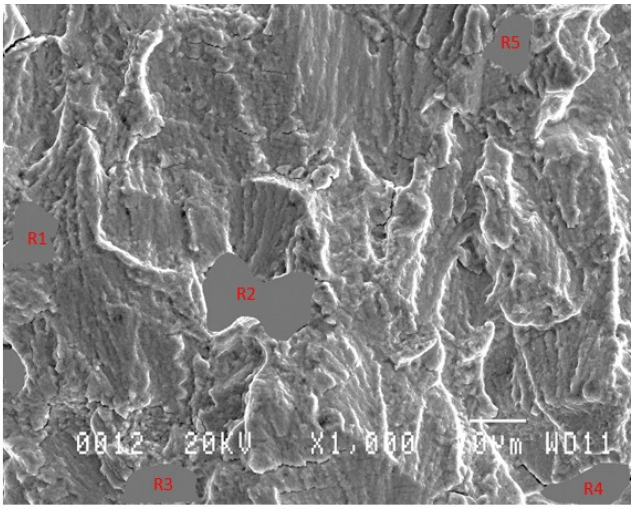

18b)

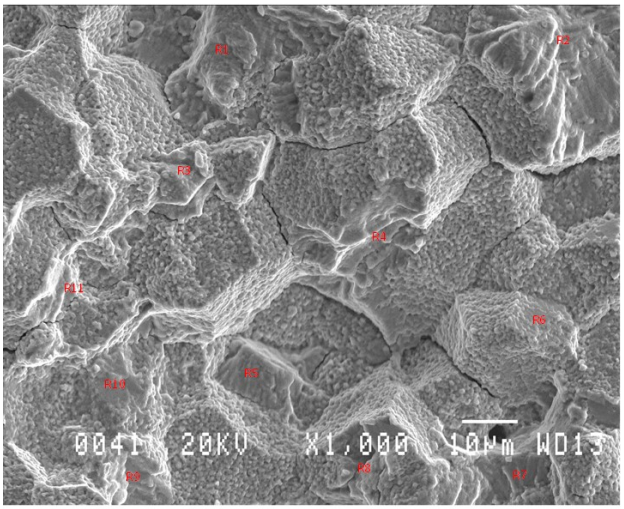

18c)

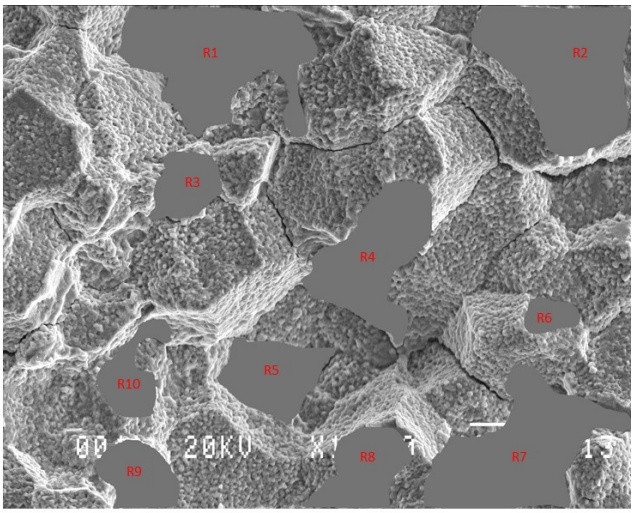

18d)

Figure 18. Measurement of intergranular failure mode content for a constant ΔK segment tested at 0.333 Hz (FC+2SA + 815°C/440h) (a and b) and FC, No Age (c and d). Intergranular failure regions indicated in a). Same regions grayed out in b) ≈ 5.3%. Transgranular failure content in c); regions grayed out in d). transgranular content subtracted to obtain intergranular content for c) ≈ 73%.

The initial results of the analysis, presented in Table III, showed that the failure mode, even at the lowest frequency was still predominantly transgranular (≈ 90 %). This narrow range of intergranular failure content made it difficult to accurately assess its effect on Paris region FCG rates. Thus two additional constant ΔK tests were performed under identical test conditions

using LSHR heat treatments which have been shown in an earlier study to be much more susceptible to environmental damage (17). It should be noted that in the earlier work it was demonstrated that in vacuum all three heat treat conditions produce very similar FCG response and thus any differences in FCG behavior observed in ambient air can be assumed to be due to environmental degradation.

For these two alternate heat treatments, the content of intergranular failure was determined for the 0.333 Hz test segments using the same procedure as described earlier so that the regions with the highest amount of intergranular failure mode could be included in the study. The microstructural characteristics and heat treat details for all three conditions were presented in a previous publication (17). The key attribute that made them useful tools in the present study was their varied resistance to environmental attack promoting intergranular crack growth. The two heat treatments shown to be susceptible to this environmental damage were: 1) Fast cool from solution (202°C/min) followed by two step age (855°C/4h +775°C/8h) + 815°C/2020hr exposure; and 2) Fast cool (202°C/min) with no subsequent aging or high temperature exposure.

The measured amount of intergranular failure for all three heat treatments is shown in Table III together with the measured FCG rates for these constant ΔK segments. Both of the alternate heat treatments resulted in a much larger degree of intergranular failure. The fast cool and no age condition resulted in an approximately 75% intergranular failure content (Fig. 18 c and d) while the FC+2SA+815°C/2020h resulted in ≈ 34% intergranular failure. The relationship between the percentage of intergranular failure mode and the measured FCG rates are shown in Fig. 19. In order to highlight the effect of environment, the FCG rates were normalized by the FCG rates measured in vacuum for tests performed under the same conditions.

Table III. Paris regime intergranular failure content in LSHR tested at 704°C					
Specimen	**Heat Treat= Cool Rate; Age; Exposure**	**Test Frequency**	**Measured % of Intergranular Failure; Avg; St. Dev.**	**Measured da/dN m/cycle (25 MPa $m^{1/2}$)**	**Predicted da/dN (Rule of Mixtures)***
V4-L14FC2	202°C/m; 855°C/4h+775°C/8h; 815°C/440h	0.333	Avg = 10.5; SD =4.4	3.90E-07	3.50E-07
V4-L14FC2	202°C/m; 855°C/4h+775°C/8h; 815°C/440h	2	Avg = 7.5; SD = 2.9	2.70E-07	3.00E-07
V4-L14FC2	202°C/m; 855°C/4h+775°C/8h; 815°C/440h	10	Avg = 0.8; SD= 0.47	1.60E-07	1.60E-07
W2-L19FC2	202°C/m; 855°C/4h+775°C/8h; 815°C/2020h	0.333	Avg=34.3; SD=4.8	1.00E-06	8.40E-07
V4-L22FC	202°C/m; No Age; No Exp.	0.333	Avg 75.3; SD=3.6	1.20E-06	1.70E-06
* Predicted FCG at 25 MPa sq m=(fraction of Intergr. Failure)*(2.2e-6 m/cycle)+(1-fraction of Intergr. Failure)*(1.45e-7 m/cycle)					

The results are striking. The intergranular failure content has a very significant effect on the measured FCG behavior. For the specimen for which the intergranular content was measured at all three test frequencies, the 10 Hz segment which produced a very negligible amount of intergranular failure (0.8%) showed similar FCG rates to the vacuum specimen. However, the 0.333 Hz segment of the same test, resulted in a 10% intergranular failure content, and produced FCG rates 2.5 times faster than the vacuum test. At a 34% intergranular failure content, for the specimen given the 815°C/2020 h exposure, the crack growth rates were 6.8 times faster than in vacuum and finally for the fast cool + no age condition, the resulting FCG rates were 11.7 times greater, with this condition exhibiting approximately 75% intergranular failure content. Based on a linear fit of the data, it is estimated that a 50% intergranular failure would produce at 704°C approximately a 8.3 fold increase in crack growth rates compared to a purely transgranular failure mode. With the caveat that data extrapolation is always risky, extrapolating the linear fit to a 100% intergranular failure resulted in an estimate of $2.2x10^{-6}$ m/cycle at ΔK of 25 MPa√m which is 15.7 times faster than a fully transgranular failure.

It is intriguing that the relationship between percent of intergranular failure and the corresponding increase in the FCG rates appears to be linear. Thus once the necessary conditions are reached for the change to an intergranular failure mode to take place, it does not matter whether these grain boundaries were previously more resistant or less resistant to

intergranular failure, their contributions to increasing the FCG rates are the same as long as amount of additional intergranular failure is also the same.

As seen in Fig. 19, the amount of intergranular failure is the dominating factor controlling the FCG behavior and thus heavily outweighing the contribution of the transgranular failure mode content. To explain this dominance of the intergranular failure mode, we can envision two failure modes co-existing with one being highly brittle and providing little resistance to crack growth while the ductile failure mode produces much higher crack growth resistance. Since the brittle failure is confined to very narrow grain boundary channels, the crack extension by micro-cracking consumes very little strain energy, while the ductile failure mechanism requires much larger amounts of strain energy, consumed through cyclic plasticity, in order for the crack to advance. Thus the failure process requiring the lowest amount of strain energy becomes dominant.

By subtracting out the contribution of the transgranular failure mode from the total cyclic crack growth rate, the relationship between the percent of intergranular failure and the magnitude of FCG caused by environmental degradation was determined. The results of this exercise are shown in Fig. 20a. Due to the linearity of the relationship between the extent of intergranular failure and the change in the FCG rates, a simple rule of mixtures can be used to predict FCG rates at a given test condition. The data in Fig. 20a was extrapolated to determine the FCG rate for a fully intergranular failure mode to obtain a value of 2.2×10^{-6} m/cycle, while a value of 1.45×10^{-7} m/cycle was used to represent fully transgranular failure (vacuum FCG rate). The predictions of the FCG rates based of the rule of mixture calculations are shown in Fig. 20b and in Table III. As seen, the limited available data are in good agreement with the predictions.

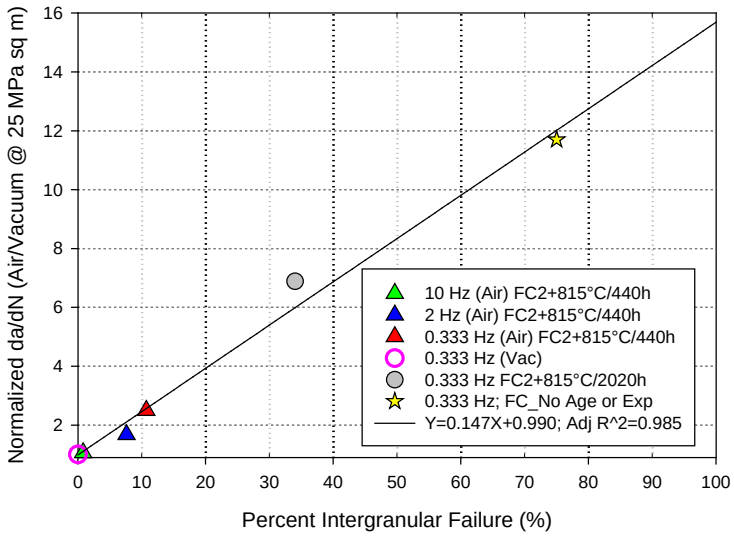

Figure 19. The relationship between the intergranular failure content of the three heat treatments utilized and the normalized FCG rates.

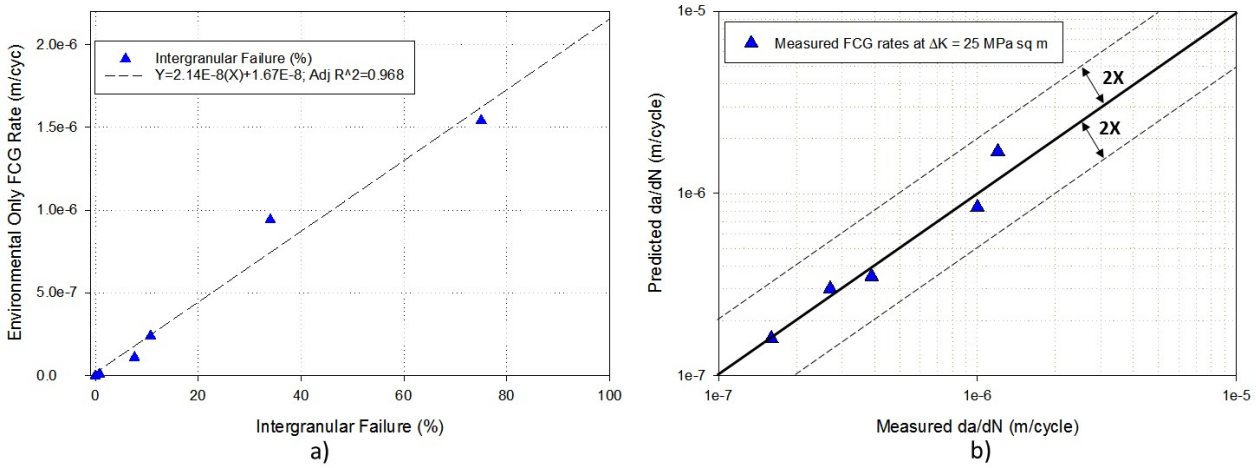

Figure 20. Relationship between intergranular failure content and the increase in the FCG rate due to environmental degradation (a) and the rule of mixtures prediction of the crack growth rates (b).

Further work is necessary to fully understand the nature and trends of these contrasting regimes of crack growth, and how they can be leveraged to enhance crack growth life prediction models. The grain boundary embrittlement process which results in the intergranular failure mode component of the Paris regime mixed mode failure has not as yet been investigated. Since it results in much different FCG behavior, it is possible that the morphology of this embrittlement process differs substantially from that which occurs in the near-threshold intergranular failure regime. We will be studying this process in the near future.

5.0 Summary and Conclusions

Cyclic near-threshold FCG behavior of two disk superalloys was evaluated, and was shown to exhibit an unexpected sudden failure mode transition from a mostly transgranular failure mode at higher stress intensities to an almost completely intergranular failure mode in the threshold regime. The change in failure modes was associated with a crossover effect in which the conditions which produced ***higher*** FCG rates in the Paris regime resulted in ***lower*** FCG rates and increased ΔK_{th} values in the threshold region. High resolution scanning and transmission electron microscopy was used to carefully characterize the crack tips at these near-threshold conditions. To contrast with the threshold failure mode regime, a quantitative assessment of the role of the failure mode on measured cyclic FCG behavior in the Paris regime was also performed.

1) Near threshold, the change in the failure mode is driven by environmental factors which allow a formation of a protective stable crack tip oxide, which decreases the crack advancement process by limiting oxygen embrittlement. Here, an intergranular oxide micro-cracking process by which crack growth occurs is mostly controlled by K_{max} parameter, with the cyclic ΔK having a secondary influence.

2) High resolution STEM-EDS analysis found the earliest oxide to nucleate along grain boundaries to be alumina. In time, the alumina begins to enter the surrounding microstructure attacking the nearest γ′ precipitates. As the Al becomes depleted near the crack, a film of Ti or Cr oxidation forms along the grain boundary depending which phase (γ or γ′) is nearest. The stable oxides protect the crack tip intergranular region from early formation of deleterious nickel-oxides as evidenced by non-oxidized Ni and Co metal being present among the oxides at these grain boundaries.

3) In contrast, for the Paris regime the percentage of intergranular cracking during mixed mode failure substantially ***increases*** FCG rates. It is estimated that a failure mode consisting of equal percentages of the two types of failure modes would result in an 8 fold increase in FCG rates, in comparison to solely transgranular failure.

4) The relationship between percent of intergranular failure and the corresponding increase in the FCG rates in the Paris regime appears to be linear. It does not matter whether the grain boundaries involved in failure were previously more resistant or less resistant to intergranular failure, their contributions to increasing the FCG rates are the same as long as amount of additional intergranular failure is also the same. Based on the linearity of the relationship, a simple rule of mixtures can be successfully used to predict the measured FCG rates.

Acknowledgement

This work supports the objectives and goals of NASA's Advanced Air Transportation Technology Project funded by the Aeronautics Research Mission Directorate.

References

1. J. Telesman, T.M. Smith, T.P. Gabb, A.J. Ring, Materials Science & Engineering A, 798, 2017, 336-350.

2) J.L. Yuen, P. Roy and W.D. Nix, Met. Trans. A, Vol. 15A, Sept. 1984, 1769-1775.

3) M.A. Hicks and J.E. King, Int. J. of Fatigue, Vol 5, No 2, April 1983, 67-74.

4) A. Shyam, S. Padula, S. Marras and W. Milligan, Met. and Matls. Trans. A, Vol 33A, July 2002, 1949-1962.

5) H.Y. Li, J.F. Sun, M.C. Hardy, H.E. Evans, S.J. Williams, T.J.A. Doel and P. Bowen, Acta Mat. 90, 2015, 355-369.

6) S. Suresh, G.F. Zamiski and R.O. Ritchie, Met. Trans. A, Vol 12A, August 1981, 1435-1443.

7) R. Molins, G. Hochstetter, J.C. Chassaigne and E. Andrieu, Acta. Mat. 45, 1997, 663-674.

8) R. Molins, J.C. Chassaigne and E. Andrieu, Materials Science Forum, Vols. 251-254, 1997, 445-452.

9) E. Andrieu, G. Hochstetter, R. Molins and A. Pineau, Oxidation Mechanisms in Relation to High Temperature Fatigue Crack Growth Properties of Alloy 718, Proc of Superalloys 718, 625, 706 and Various Derivatives, Edited by E.A. Loria, TMS, 1994, 619-631.

10) L. Viskari, M. Hornqvist, K.L. Moore, Y. Cao, K. Stiller, Intergranular crack tip oxidation in a Ni-base superalloy, Acta Materialia, Vol 61, Iss. 10, 2013, 3630-3639.

11) P.F. Browning, Time Dependent Crack Tip Phenomena in Gas Turbine Disk Engines, PhD Thesis, Rensselaer Polytechnic Institute, 1998.

12) N. Birks, G.H. Meier, and F.S. Pettit, Introduction To The High-Temperature Oxidation of Metals, 2nd Eds.,Cambridge University Press, 2006.

13). J.L. Smialek and G.H. Meier, in Superalloys II ed by C.T. Sims et al, Wiley-Interscience, 1987, 293-326.

14) T. Mura, A theory of fatigue crack initiation, Matls. Science and Eng. A, 176, 1994, 61-70.

15) K.S. Chan, Time-Dependent Crack Growth Thresholds of Ni-Base Superalloys, Metallurgical and Materials Transactions A, Vol 45, Issue 8, 2014, 3454-3466.

16) R.O. Ritchie, Int. J. of Fracture, 100, 1999, 55-83.

17) J. Telesman, T.P. Gabb, L.J. Ghosn in Superalloys 2016, ed M. Hardy et al, TMS, 2016, 551-560.